Article

Cortical Firing and Sleep Homeostasis

Vladyslav V. Vyazovskiy, Umberto Olcese, Yaniv M. Lazimy, Ugo Faraguna, Steve K. Esser, Justin C. Williams, Chiara Cirelli, and Giulio Tononi

Supplemental figures

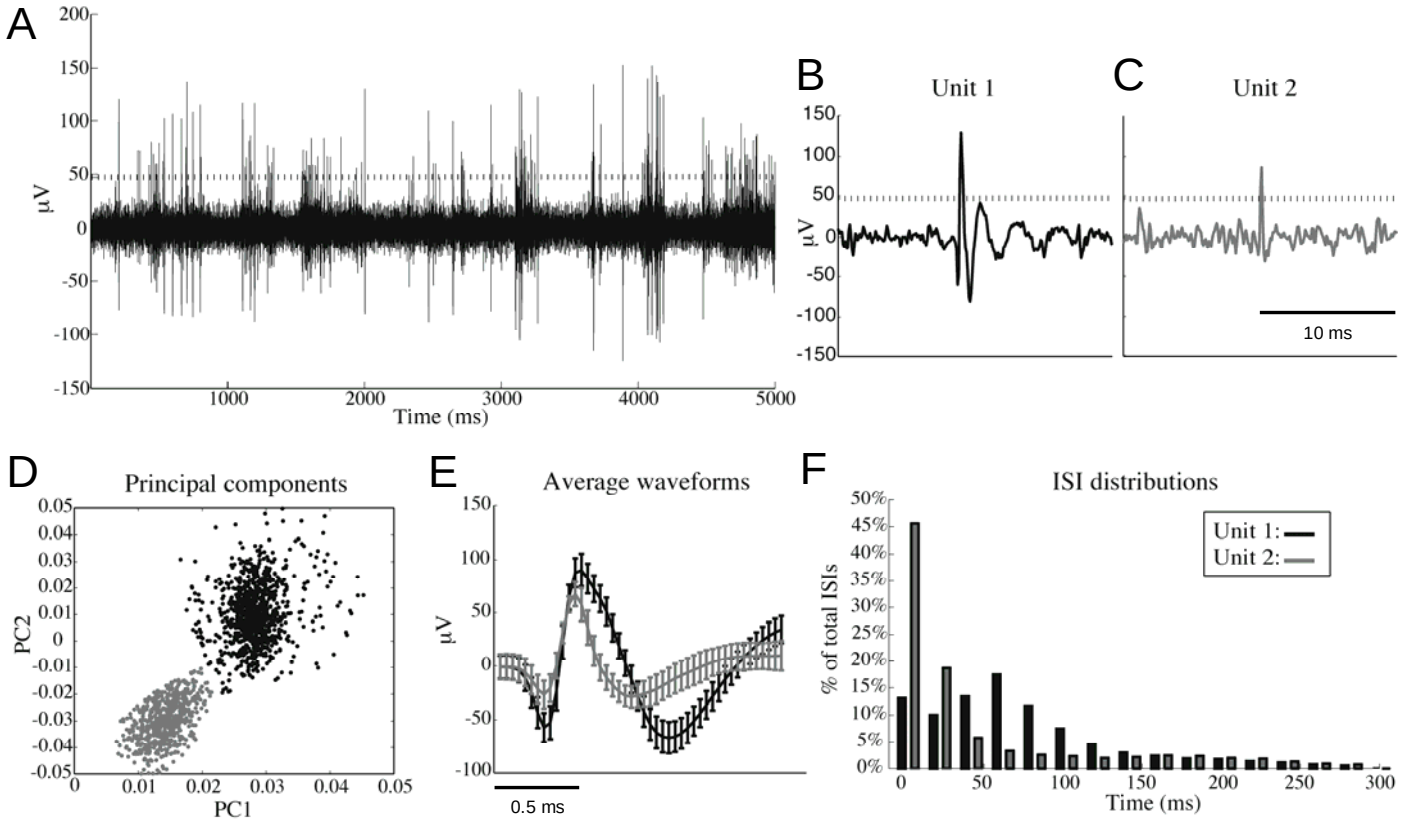

Supplemental Figure 1. Spike sorting
(A) Raw multiunit activity (MUA) recorded from one channel in one individual rat. Horizontal line depicts the amplitude threshold for spike detection. Note that the level of noise was significantly below the amplitude of the spikes. (B-C) Two units could be isolated in this channel, based on different amplitude and shape of their waveform. (D-E) Spike sorting using principal component analysis revealed two distinct clusters, corresponding to the two individual units (panel E: mean values ± standard devation). (F) The two detected units have different patterns of firing, as indicated by the distribution of their interspike intervals (ISI).

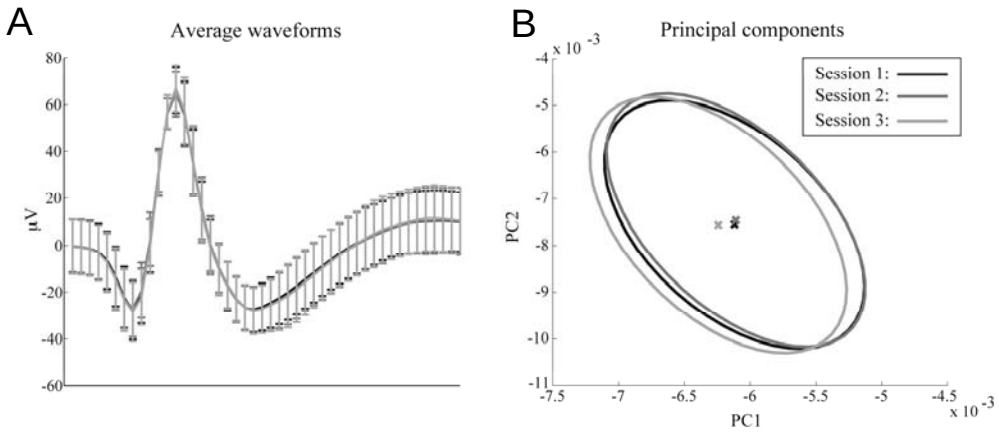

Supplemental Figure 2. Spike stability
(A) Average spike waveforms of a representative unit during three consecutive recording sessions separated by ~ 2 hours. Mean values ± standard deviation. Note that the spike waveforms are stable. (B) Distribution of the values of the first two principal components of the waveforms from a single sorted neural unit, represented as an ellipse whose center and radius are at the mean and standard deviation of the distribution, respectively.

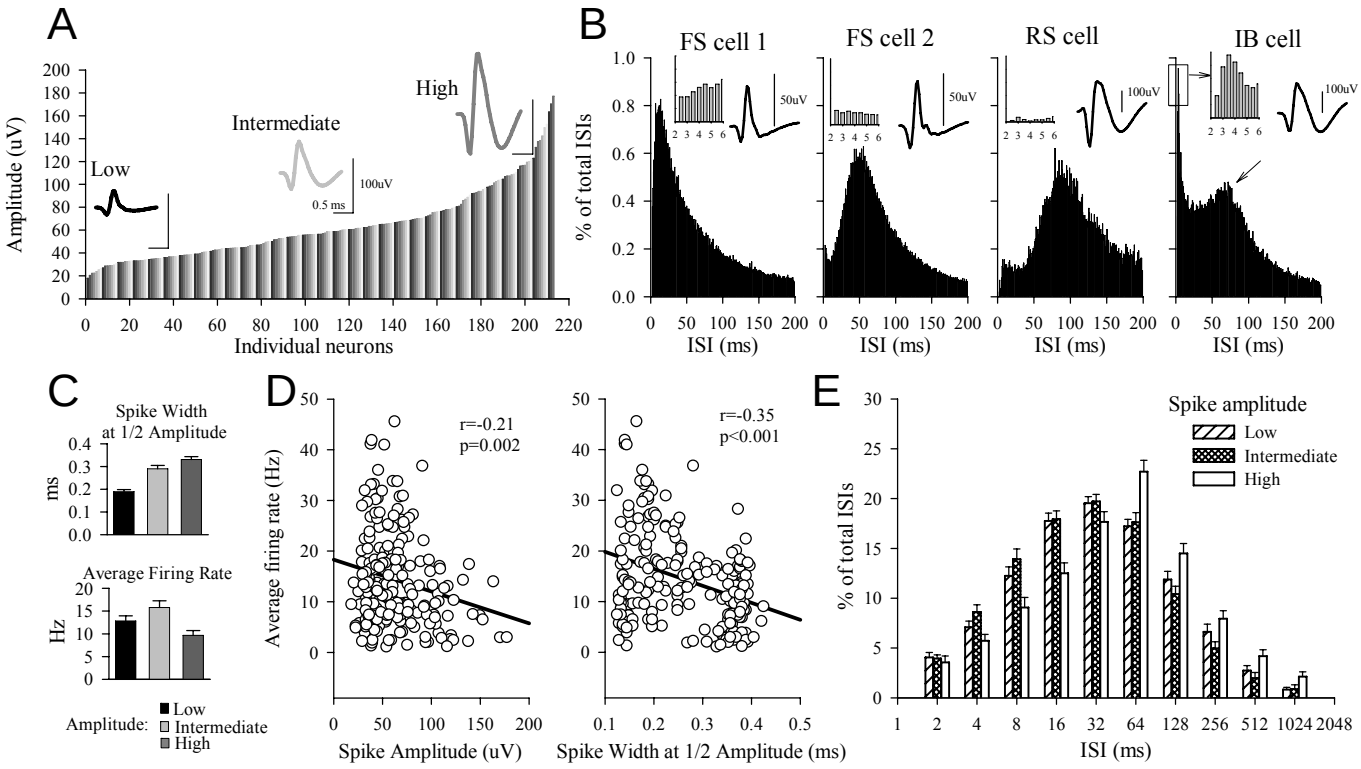

Supplemental Figure 3. Characterization of individual recorded units.
(A) All units recorded from the barrel cortex in the present study (n=213, n=6 rats) sorted in ascending order as a function of spike amplitude. Average waveforms for the lowest, intermediate and largest 20% of spike amplitudes are shown above the bars. (B) Interspike intervals (ISIs) distribution and average waveform for four representative neurons belonging to three major firing phenotypes, putative fast spiking (FS), putative regular spiking (RS) and putative intrinsically bursting (IB). Insets show the shortest ISIs (<6 ms) to highlight the bursting pattern of IB neuron discharge. (C) Mean values (±SEM) of spike width at ½ amplitude and corresponding average firing rate for neurons with the lowest, intermediate and largest 20% of spike amplitude. (D) Relationship between spike amplitude and spike width and average firing rates. (E) Average ISI histogram for neurons with the lowest, intermediate and biggest 20% of spike amplitude plotted as a function of the logarithmically increasing ISI ranges (mean values + SEM, n=6 rats, 213 neurons).

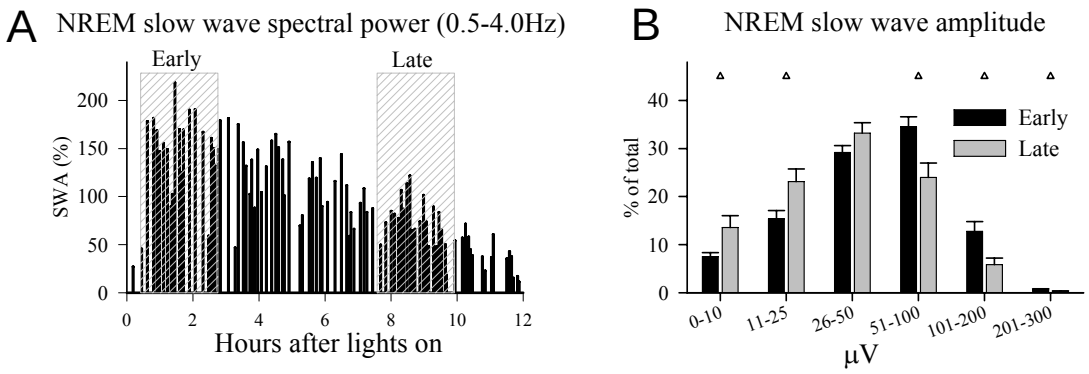

Supplemental Figure 4. Early sleep is associated with more frequent occurrence of high-amplitude EEG slow waves

(A) SWA profile during the major sleep phase (light period) in one representative rat (mean SWA intraepisodic values expressed as % of the 12-hour light period mean). (B) Distribution of the amplitude of slow waves in early and late sleep. The number of waves was computed for 6 amplitude ranges (0-300 μV). Mean values (+ SEM, n = 6 rats) are plotted as % of all waves (triangles, $p<0.05$, paired t-test).

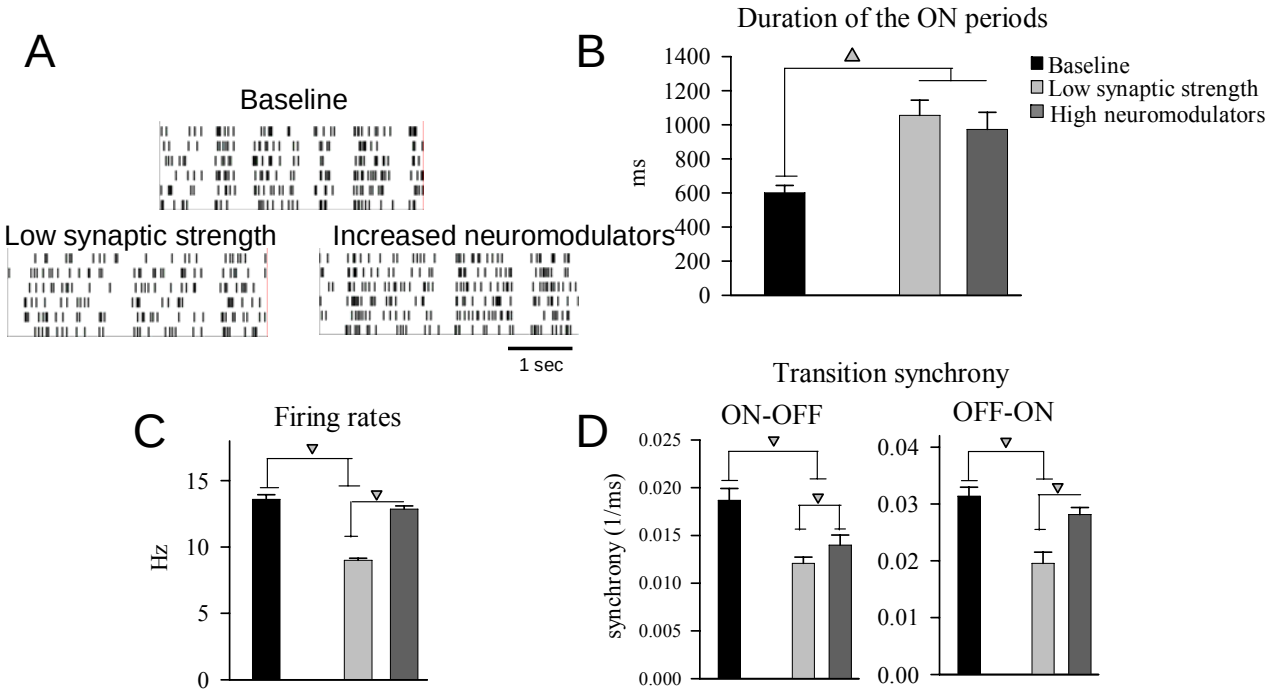

Supplemental Figure 5. Comparison of the effects of changes in synaptic strength and in the levels of neuromodulators on neural activity during sleep in a large-scale model of the thalamocortical system

A large-scale model of thalamocortical system was used to investigate whether changes in synaptic strength or neuromodulators can account for the changes in neuronal firing rates and synchrony reported in the paper (the model is based on Esser et al., 2007 and Hill and Tononi, 2005 and is described in detail in Supplemental Experimental Procedures). (A,B) The increased levels (by 25%) of arousal-promoting neuromodulators in the sleep condition resulted in a pattern of activity similar to that obtained by decreasing synaptic strength (by 25%) in a random sample (33%) of excitatory corticocortical connections. (C,D) A decrease in firing rates and neuronal synchrony at the OFF-ON transition was apparent only after lowering synaptic strength. Neuronal synchrony at the ON-OFF transition was reduced significantly more as a result of lowering synaptic strength compared to increasing neuromodulation. Values are mean +SEM (20 neurons); triangles, $p<0.05$, paired t-test.

.

Supplemental Experimental Procedures

Surgery and multiunit activity recording

Male WKY rats (n=7, Charles River, 11-12 week old at time of surgery) were used. Under deep isoflurane anesthesia (1.5-2 % volume), rats were implanted in the left barrel cortex (n=6, B: -2-3 mm, L: 2-3 mm) or in the frontal cortex (n=1, B: +1-2 mm, L: 2-3 mm) with 16-ch (2x8) polyimide-insulated tungsten microwire arrays (Tucker-Davis Technologies Inc, Alachua, FL, wire diameter 33μm, electrode spacing 175μm, row separation L-R: 500μm; D-V: 1mm) according to the "Surgical implantation guidelines" (Neuronexus Technologies, Inc.) and (Kralik et al., 2001). One day before surgery animals received an i.p. dose of dexamethasone (Dex) to suppress local immunological response (0.2mg/kg), and subsequently Dex was given with food pellets every day for the duration of the experiment.

The surgical procedure was performed in sterile conditions, using Ethylene Oxide sterilized materials. A ~ 2 mm craniotomy was made using first a 1.4mm drill bit and then a 0.7mm drill bit, with the aid of an high-speed surgical drill. The hole was adjusted to the size of the array by removing the remaining fragments of the bone with a Friedman-Pearson Rongeur (part number 16221-14, FST). In most cases the removal of the dura did not cause bleeding (when bleeding occurred, it was stopped with gelfoam soaked in sterile saline). The dura was dissected with vitrectomy scissors (2.2 mm straight blades, part number 15036-14, FST).

The electrode array was advanced into the brain tissue by penetrating the pia mater, making an effort to avoid vascular damage (Bjornsson et al., 2006). Electrode insertion was achieved by advancing the electrode array until both the superficial and the deep rows of the arrays were under the cortical surface. The final position of the array was adjusted by withdrawing or lowering it slowly (~100 μm steps) until most channels showed robust single- or multiunit activity. The final insertion depth was ~1.2 mm below the pial surface for the deep row (layer V), and ~ 0.2 mm for the superficial row (layer II-III). Warm (40ºC) agarose gel mixed with Dex (0.2%) was gently placed around the array to fill the craniotomy. At this stage special care was taken to avoid displacing the array in the horizontal dimension. The two-component silicon gel (KwikSil; World Precision Instruments, FL, USA) was used to seal the craniotomy and protect the surface of the brain from dental acrylic. After ~10 min, required for the gel to polymerize, dental acrylic was gently placed around the electrode, fixing the array to the skull. The ground electrode was placed above the cerebellum and additional anchor screws were placed bilaterally in the frontal bone. After surgery all rats were housed individually in transparent Plexiglas cages (36.5 x 25 x 46 cm). Lighting and temperature were kept constant (LD 12:12, light on at 10am, 23±1°C; food and water available ad libitum and replaced daily at 10am). About a week was allowed for recovery after surgery, and experiments were started only after the sleep/waking cycle had fully normalized. Animal protocols followed the National Institutes of Health Guide for the Care and Use of Laboratory Animals and were in accordance with institutional guidelines.

Signal processing and analysis

Data acquisition and online spike sorting were performed with the Multichannel Neurophysiology Recording and Stimulation System (Tucker-Davis Technologies Inc., TDT). Spike data were collected continuously (25 kHz, 300-5kHz), concomitantly with the local field potentials (LFPs) from the same electrodes (256 Hz) and surface EEG (256 Hz). Amplitude thresholds for online spike detection were set manually based on visual and auditory control and allowed only cross-

ings of spikes with signal-to-noise ratio of at least two. Since extracellular multiunit (MUA) signals are usually asymmetric, the detection threshold was applied to the side where spike waveforms exhibited greater deflection (Rasch et al., 2008). Whenever the recorded voltage exceeded a predefined threshold (~20-30 μV), a segment of 46 samples (0.48 ms before, 1.36 ms after the threshold crossing) was extracted and stored for later use together with the corresponding time stamps. The online spike sorting was performed with OpenEx software (TDT), by applying a voltage window through which the signal must pass under visual and auditory control. Such thresholding allowed excluding the low-amplitude noise and most of high-amplitude artifacts related to chewing and grooming. Spike data were then subjected to offline sorting procedure (see below). The amplitude thresholds used in our study were sufficiently low to enable us to record several neuronal subpopulations (Figure S3). To avoid contamination of the sorted units, especially of small amplitude, by multiunit activity, all individual neurons were carefully screened: units showing relatively high proportion (>1-2 %) of short refractory periods (<2.5 ms) and no major peaks on the distribution of ISIs were discarded from the analysis.

The EEG power spectra were computed by a Fast Fourier Transform (FFT) routine for 4-sec epochs (0.25 Hz resolution). Detection of individual slow waves was performed on the EEG signal after band pass filtering (0.5-4 Hz, stopband edge frequencies 0.1-10 Hz) with MATLAB filtfilt function exploiting a Chebyshev Type II filter design (MATLAB, The Math Works, Inc., Natick, MA) (Achermann and Borbely, 1997). Filter settings were optimized after visual observation to obtain the maximal resolution of wave shape, as well as the least intrusion of faster (e.g. spindle) activities. Slow waves were detected as negative deflections of the EEG signal between two consecutive positive deflections above the zero-crossing separated by at least 0.1 sec (Vyazovskiy et al., 2007). The first segment of the slow wave (from the first positive peak to the minimal negative peak) and the second segment (from the minimal negative peak to the second positive peak) were detected and their slopes were calculated as mean first derivatives.

For staging, signals were loaded with custom-made Matlab programs using standard TDT routines, and subsequently transformed into the EDF (European Data Format) with Neurotraces software. Sleep stages were scored off-line by visual inspection of 4-sec epochs (SleepSign, Kissei), where the EEG, LFP, EMG and spike activity was displayed. Waking was characterized by low voltage, high frequency EEG pattern and phasic EMG activity. Epochs of eating, drinking and intense grooming were usually excluded, since during those periods MUA was contaminated by muscle artifacts, precluding reliable isolation of individual spikes. NREM sleep was characterized by the occurrence of high amplitude slow waves and low tonic EMG activity (Figure 1). During REM sleep the EEG was similar to that during waking, but only heart beats and occasional twitches were evident in the EMG signal. Epochs containing artifacts, predominantly during active waking, were excluded from spectral analysis. Vigilance states could always be determined.

Both sleep and waking were significantly more fragmented in the dark period compared to the light phase. Specifically, in the dark compared to the light period, there was an increase in brief (≤ 16sec) awakenings during sleep (n / 1hour of NREM sleep: Light: 36.8±0.3, Dark: 44.1±0.4, n=7 rats; $p<0.01$, unpaired t-test), as well as in the number of short sleep attempts (NREM episodes ≤ 16sec; n / 1hour of NREM sleep: Light: 14.5±0.2, Dark: 24.7±0.4, n=7 rats; $p<0.01$, unpaired t-test). Vigilance states showed the expected differences in average firing rates (Hobson and McCarley, 1971; Noda and Adey, 1973; Steriade et al., 2001), with lower mean firing rates in NREM sleep compared to both waking and REM sleep (Figures 2,6). Of note,

vigilance states also differed in the overall distribution of ISIs (Figure 2C). Moreover, firing rates during the ON periods were significantly higher than average firing rates in NREM sleep ($p<0.01$).

Experimental design

Recordings were performed continuously for 2-3 weeks starting from day 5 after surgery, when rats appeared normal and their sleep-wake cycle had normalized. A total of 4-7 animals contributed to different experiments and data analyses. To assure that the homeostatic changes were consistent between days, at least one 12-hour light period and one 12-hour dark period (range: 1-7 days) were selected per animal based on signal stability, and analyzed separately. After 2-3 stable baselines, one or two 4-h sleep deprivation (SDep) experiments were performed in each animal (at least 5 days apart), each followed by an undisturbed recovery period. SDep began at light onset and involved continuous observation of the animal and its polysomnographic recording. When the animal assumed a sleep posture, or started exhibiting electrographic signs of drowsiness (slow waves or low tone EMG), it was given a novel object to play with, or was activated by acoustic stimuli (e.g. tapping on the cage). Rats were not touched or handled directly. Objects included paper tissue and paper towels, bedding material transferred from another cages, and toys of various shape and size. Rats were never disturbed when they were spontaneously awake, feeding or drinking.

For analysis of the firing rates within the ON periods during the night, the longest artifact-free uninterrupted episode of NREM sleep (at least 1-2 min long) was selected based on the immediately preceding sleep-wake history (after W vs. after S, see Figure 6A). For the analysis of the firing rates within the ON periods during the day, the longest artifact-free uninterrupted episode of NREM sleep (at least 2-3 min long) was selected in early (hour 1 after lights on) and late (~ 5-6 h after lights on) sleep (Figure 6B). Total average firing rates (including the ON and OFF periods) during sleep were compared between the first and last 3-hour intervals of the light period (high and low sleep pressure): NREM sleep, 32.2± 9.3 min and 23.5±8.9 min; REM sleep, 9.2±2.5 min and 8.1±2.5 min, respectively (Figure 6D). For waking, firing rates were compared between episodes lasting >10 min, preceding and following (high and low sleep pressure, respectively) consolidated sleep episodes lasting > 10 min, and consisting of at least 70% of NREM sleep.

Data processing and analysis

In naturally sleeping animals extracellular recordings in the visual or somatosensory neocortex reveal periods of synchronous activity among neuronal populations, interrupted by periods of population silence of variable duration (e.g. (Ji and Wilson, 2007; Luczak et al., 2007)). Consistently, we observed similar periods of generalized neuronal activity (ON-periods) and silence (OFF-periods) in our recordings from the barrel cortex (e.g. Figure 1E). To detect such ON and OFF periods, as a first step all time stamps corresponding to individual spike occurrences were concatenated across all recording channels showing robust single- or multiunit activity (on average ~10 channels per animal). Next, onset and offset of the periods with no unit activity were identified. Such silent periods were referred to as OFF periods if they lasted at least 50 ms. In all cases (both in early and late sleep) the beginning of the OFF periods was defined as the time when the last unit of the population stopped firing, whereas the end of the OFF periods was defined as the time when at least one unit out of the entire population resumed activity. Similarly, in all cases the beginning and end of the ON periods were detected if at least one unit out of the

entire population resumed or stopped activity, respectively. The criterion for the minimal duration of the OFF periods was optimized based on the observation that OFF periods lasting longer than 50 ms were reliably associated with a clear-cut negative slow wave in the simultaneous EEG recordings (Figure 3B). However, varying the minimal duration criteria for the OFF periods revealed that the effects of sleep-wake history were robust, provided that the OFF periods were not too short (≤ 10 ms). The ON periods were defined as intervals of sustained unit firing lasting between 50-4000 ms, and consisting of at least 10 spikes. The average duration of the ON periods was 815.5 ± 119.9 ms, whereas the OFF periods lasted on average 85.8 ± 5.9 ms (n=6 rats), similar to what previously reported in the visual cortex (Ji and Wilson, 2007). Prior to computing averages, the incidence of both the ON and OFF periods was expressed per 1 min of NREM sleep to correct for daily variations in total sleep time. The values are expressed as % of 12-hour mean to emphasize the relative magnitude of the homeostatic change from early to late sleep and facilitate comparison with other studies. Note that the absolute values for the number and duration of ON and OFF periods for the individual rat depicted in Figure 4C,D are close to the sample average. Note also that the number of OFF periods slightly exceeds the number of ON periods due to the minimal criteria used for their detection. ON periods were defined as sequences of at least 10 spikes with a maximal inter-spike timing < 50 ms, thus excluding periods with low and scarce neuronal activity (Luczak et al., 2007; Volgushev et al., 2006). On the other hand, only periods of silence > 50 ms were called OFF periods, and the occurrence of one single spike was sufficient to terminate an OFF period. For the analysis of firing rates within the ON periods, only consolidated (> 20 ms) periods of sustained activity not interrupted by OFF periods > 20 ms, and preceded and followed by a negative EEG slow wave within 150 ms, were included. Such criteria were optimized based on the visual inspection of the individual records of each animal, but detection of the ON periods based on the minimal duration of 50 ms (as above) yielded similar results. Computation of neuronal synchrony at the ON-OFF and OFF-ON transitions was based on > 50 ms ON periods in which at least 50% of all recorded units generated at least 2 spikes.

Spike sorting

Spikes were first detected using a threshold-based technique (Figure S1). Only those spikes for which waveform shape was consistent with typical recordings and the signal/noise ratio was > 2 were considered. Principal components (PCs) were extracted (Lewicki, 1998) and clustering was performed based on the SMEM algorithm (Tolias et al., 2007; Ueda et al., 2000). This algorithm operates on Gaussian mixtures by iteratively splitting and merging Gaussian clusters, until convergence of a maximization index is reached (we employed only the split phase to reduce computational time). Although the merge step should help avoiding convergence to local maxima (Ueda et al., 2000), we empirically verified that, on our data, the split step alone was sufficient to correctly estimate the number of clusters. To obtain a satisfactory clustering quality, parameters were initialized as follows: 1) the number of PCs was set to 2 (sorting based on 3 PCs yielded similar results). Two PCs accounted on average for 55% of the total variance; 2) the threshold for the algorithm convergence was set to 0.01 (this value influences the number of detected clusters); 3) the threshold for classification was set to 0.1, i.e. all spikes with a probability < 10% of belonging to a cluster were discarded. Post hoc all clusters were checked and clusters with standard deviation > 20% of mean spike amplitude were rejected. On average 9 neurons/rat/recording session were reliably identified.

While it is often difficult to guarantee that all waveforms assigned to the same cluster originate from a single neuron, tracking waveform statistics and comparing them with functional measures can increase confidence that the recorded neural population is stable over the time period of interest. Figure S2 shows the mean and standard deviation of the values of the first two PCs calculated on the waveforms of a single sorted unit. This is represented as an ellipse whose center and radii are at the mean and standard deviations of the distribution, respectively. Carrying out this procedure on subsequent recording sessions revealed that the mean does not drift outside of the standard deviation for either of the PCs. Computation of the interspike interval histogram for single sorted units showed a unimodal distribution with a finite refractory period (Figure S1,S3). This, coupled with the PC stability, suggests that the majority of sorted neurons were from a stable population throughout the time duration of the analysis presented in this study, and that changes in the number of active units is unlikely to explain the results and findings presented.

The shape and amplitude of extracellularly recorded spikes is profoundly affected by axon geometry, inhomogeneities in the extracellular space, volume conduction or the electrode-to-neuron distance (Kole et al., 2007; Pattle, 1971; Richerson et al., 2005). Therefore, cortical neurons are usually classified into several distinct categories based not only on spike morphology, but also on their firing behavior, responses to the intracellular depolarizing current pulses, functional tuning and other criteria (Connors and Gutnick, 1990; Diaz-Mataix et al., 2006; Diester and Nieder, 2008; Gonzalez-Burgos et al., 2005; Gray and McCormick, 1996; Jung et al., 1998; Kawaguchi and Kubota, 1997; Mallet et al., 2005; McCormick et al., 1985; Povysheva et al., 2006; Puig et al., 2008; Tierney et al., 2004; Tseng et al., 2006; Valenti and Grace, 2008). In our study detected neurons belonged to different neuronal subtypes and, as expected, showed significant variability in average firing rates (Figures 7,S3). Specifically, putative fast-spiking neurons were characterized by narrow action potentials and mostly short ISIs, putative regular spiking neurons had broad spikes and relatively low firing rates, whereas putative bursting neurons also had broad spikes but exhibited 2 modes of ISIs distribution, with one mode between 3 and 4 ms (Bartho et al., 2004; McCormick et al., 1985; Steriade et al., 1993). Subdivision of the neurons into two subtypes based on spike width revealed that the effects of the sleep/wake history were similar among all neuronal phenotypes (Figure 7). This further supports the findings that neural waveform stability was not a confounding factor in determining the relationship between neural firing and sleep state.

Histological verification

Upon completion of the experiments the position of the LFP electrodes was verified by histology in all animals. After perfusion under deep isoflurane anesthesia (3% in oxygen), brains were post-fixed, rapidly frozen on dry ice, cut into 50μm serial coronal sections, and subjected to cresyl-violet (Nissl) staining. In all cases the deep row of the array was located within layer V, whereas the superficial row was in layers II-III.

Description of the model

The large-scale computational model of the thalamocortical system we used is similar to the one previously described (Esser et al., 2007; Hill and Tononi, 2005) (Figure S5), and is able to faithfully reproduce several brain phenomena, including wakefulness, sleep and transcranial magnetic stimulation. Briefly, the model is composed of 3 granular cortical regions hierarchically connected (from area 1 to area 3). Each region consists of three layers (layer II-III, layer IV and

layer V-VI) and has correspondent thalamic and reticular areas. Layers are 30 by 30 grids, each grid point containing 2 excitatory neurons and an inhibitory one. Connections between neurons have been modeled to be as realistic as possible. Single connections are established randomly using a Gaussian spatial density profile (details in (Esser et al., 2007; Hill and Tononi, 2005)).

Neurons are modeled as single-compartment spiking neurons with Hodgkin−Huxley-style currents. Their subthreshold membrane potential is governed by the following equation:

$$\frac{dV}{dt} = \left(-g_{NaL}\left(V - E_{Na}\right) - g_{KL}\left(V - E_K\right) - I_{syn} - I_{\text{int}}\right) \Big/ \tau_m ,$$

where V is the membrane potential, g_{NaL} and g_{KL} are the sodium and potassium leakage conductances, E_{Na} and E_K are the sodium and potassium reversal potentials, I_{syn} and I_{int} are the sums of all synaptic and intrinsic currents, τ_m is the membrane time constant. The resting membrane potential is mainly determined by the sodium and potassium leak conductances. When V reaches or exceeds a threshold a spike is generated, then intrinsic currents regulate the membrane potential. Intrinsic currents include a non-inactivating hyperpolarization-activated cation current I_h, a low-threshold fast-activating calcium current I_T, a persistent sodium current $I_{Na(p)}$ and a depolarization activated potassium current I_{DK}. Four kinds of synaptic channels are present: NMDA, AMPA, $GABA_A$ and $GABA_B$. The sum of all synaptic currents I_{syn} is modeled as follows:

$$I_{syn} = \sum_{i,j} g_j^{(i)}\left(V - E_j\right),$$

where *i* represents the i^{th} channel present on the cell and *j* stands for the kind of synaptic channel. By changing conductance values it is possible to linearly modulate the strength of each synapse. The effect of the neuromodulatory systems is modeled by changing conductance values, therefore mimicking the final effects of neuromodulators rather than their dynamics. By changing conductances it is also possible to modulate the vigilance state of the network, switching from the waking to the NREM sleep modality, as shown in detail in (Esser et al., 2007; Hill and Tononi, 2005). Spontaneous activity is obtained by implementing sparse connections to randomly activating sub-cortical regions. “Minis” (spontaneous miniature synaptic currents) are also present in the model as low threshold PSPs.

Supplemental References

Achermann, P., and Borbely, A. A. (1997). Low-frequency (< 1 Hz) oscillations in the human sleep electroencephalogram. Neuroscience *81*, 213-222.

Bartho, P., Hirase, H., Monconduit, L., Zugaro, M., Harris, K. D., and Buzsaki, G. (2004). Characterization of neocortical principal cells and interneurons by network interactions and extracellular features. J Neurophysiol *92*, 600-608.

Bjornsson, C. S., Oh, S. J., Al-Kofahi, Y. A., Lim, Y. J., Smith, K. L., Turner, J. N., De, S., Roysam, B., Shain, W., and Kim, S. J. (2006). Effects of insertion conditions on tissue strain and vascular damage during neuroprosthetic device insertion. J Neural Eng *3*, 196-207.

Connors, B. W., and Gutnick, M. J. (1990). Intrinsic firing patterns of diverse neocortical neurons. Trends Neurosci *13*, 99-104.

Diaz-Mataix, L., Artigas, F., and Celada, P. (2006). Activation of pyramidal cells in rat medial prefrontal cortex projecting to ventral tegmental area by a 5-HT1A receptor agonist. Eur Neuropsychopharmacol *16*, 288-296.
Diester, I., and Nieder, A. (2008). Complementary contributions of prefrontal neuron classes in abstract numerical categorization. J Neurosci *28*, 7737-7747.
Esser, S. K., Hill, S. L., and Tononi, G. (2007). Sleep homeostasis and cortical synchronization: I. Modeling the effects of synaptic strength on sleep slow waves. Sleep *30*, 1617-1630.
Gonzalez-Burgos, G., Krimer, L. S., Povysheva, N. V., Barrionuevo, G., and Lewis, D. A. (2005). Functional properties of fast spiking interneurons and their synaptic connections with pyramidal cells in primate dorsolateral prefrontal cortex. J Neurophysiol *93*, 942-953.
Gray, C. M., and McCormick, D. A. (1996). Chattering cells: superficial pyramidal neurons contributing to the generation of synchronous oscillations in the visual cortex. Science *274*, 109-113.
Hill, S., and Tononi, G. (2005). Modeling sleep and wakefulness in the thalamocortical system. J Neurophysiol *93*, 1671-1698.
Hobson, J. A., and McCarley, R. W. (1971). Cortical unit activity in sleep and waking. Electroencephalogr Clin Neurophysiol *30*, 97-112.
Ji, D., and Wilson, M. A. (2007). Coordinated memory replay in the visual cortex and hippocampus during sleep. Nat Neurosci *10*, 100-107.
Jung, M. W., Qin, Y., McNaughton, B. L., and Barnes, C. A. (1998). Firing characteristics of deep layer neurons in prefrontal cortex in rats performing spatial working memory tasks. Cereb Cortex *8*, 437-450.
Kawaguchi, Y., and Kubota, Y. (1997). GABAergic cell subtypes and their synaptic connections in rat frontal cortex. Cereb Cortex *7*, 476-486.
Kole, M. H., Letzkus, J. J., and Stuart, G. J. (2007). Axon initial segment Kv1 channels control axonal action potential waveform and synaptic efficacy. Neuron *55*, 633-647.
Kralik, J. D., Dimitrov, D. F., Krupa, D. J., Katz, D. B., Cohen, D., and Nicolelis, M. A. (2001). Techniques for long-term multisite neuronal ensemble recordings in behaving animals. Methods *25*, 121-150.
Lewicki, M. S. (1998). A review of methods for spike sorting: the detection and classification of neural action potentials. Network *9*, R53-78.
Luczak, A., Bartho, P., Marguet, S. L., Buzsaki, G., and Harris, K. D. (2007). Sequential structure of neocortical spontaneous activity in vivo. Proc Natl Acad Sci U S A *104*, 347-352.
Mallet, N., Le Moine, C., Charpier, S., and Gonon, F. (2005). Feedforward inhibition of projection neurons by fast-spiking GABA interneurons in the rat striatum in vivo. J Neurosci *25*, 3857-3869.
McCormick, D. A., Connors, B. W., Lighthall, J. W., and Prince, D. A. (1985). Comparative electrophysiology of pyramidal and sparsely spiny stellate neurons of the neocortex. J Neurophysiol *54*, 782-806.
Noda, H., and Adey, W. R. (1973). Neuronal activity in the association cortex of the cat during sleep, wakefulness and anesthesia. Brain Res *54*, 243-259.
Pattle, R. E. (1971). The external action potential of a nerve or muscle fibre in an extended medium. Phys Med Biol *16*, 673-685.
Povysheva, N. V., Gonzalez-Burgos, G., Zaitsev, A. V., Kroner, S., Barrionuevo, G., Lewis, D. A., and Krimer, L. S. (2006). Properties of excitatory synaptic responses in fast-spiking interneurons and pyramidal cells from monkey and rat prefrontal cortex. Cereb Cortex *16*, 541-552.

Puig, M. V., Ushimaru, M., and Kawaguchi, Y. (2008). Two distinct activity patterns of fast-spiking interneurons during neocortical UP states. Proc Natl Acad Sci U S A.
Rasch, M. J., Gretton, A., Murayama, Y., Maass, W., and Logothetis, N. K. (2008). Inferring spike trains from local field potentials. J Neurophysiol *99*, 1461-1476.
Richerson, S., Ingram, M., Perry, D., and Stecker, M. M. (2005). Classification of the extracellular fields produced by activated neural structures. Biomed Eng Online *4*, 53.
Steriade, M., Nunez, A., and Amzica, F. (1993). Intracellular analysis of relations between the slow (< 1 Hz) neocortical oscillation and other sleep rhythms of the electroencephalogram. J Neurosci *13*, 3266-3283.
Steriade, M., Timofeev, I., and Grenier, F. (2001). Natural waking and sleep states: a view from inside neocortical neurons. J Neurophysiol *85*, 1969-1985.
Tierney, P. L., Degenetais, E., Thierry, A. M., Glowinski, J., and Gioanni, Y. (2004). Influence of the hippocampus on interneurons of the rat prefrontal cortex. Eur J Neurosci *20*, 514-524.
Tolias, A. S., Ecker, A. S., Siapas, A. G., Hoenselaar, A., Keliris, G. A., and Logothetis, N. K. (2007). Recording chronically from the same neurons in awake, behaving primates. J Neurophysiol *98*, 3780-3790.
Tseng, K. Y., Mallet, N., Toreson, K. L., Le Moine, C., Gonon, F., and O'Donnell, P. (2006). Excitatory response of prefrontal cortical fast-spiking interneurons to ventral tegmental area stimulation in vivo. Synapse *59*, 412-417.
Ueda, N., Nakano, R., Ghahramani, Z., and Hinton, G. E. (2000). SMEM algorithm for mixture models. Neural Comput *12*, 2109-2128.
Valenti, O., and Grace, A. A. (2008). Entorhinal Cortex Inhibits Medial Prefrontal Cortex and Modulates the Activity States of Electrophysiologically Characterized Pyramidal Neurons In Vivo. Cereb Cortex.
Volgushev, M., Chauvette, S., Mukovski, M., and Timofeev, I. (2006). Precise long-range synchronization of activity and silence in neocortical neurons during slow-wave oscillations [corrected]. J Neurosci *26*, 5665-5672.
Vyazovskiy, V. V., Riedner, B. A., Cirelli, C., and Tononi, G. (2007). Sleep homeostasis and cortical synchronization: II. A local field potential study of sleep slow waves in the rat. Sleep *30*, 1631-1642.